Atmos. Chem. Phys. Discuss., 15, 1171–1191, 2015
www.atmos-chem-phys-discuss.net/15/1171/2015/
doi:10.5194/acpd-15-1171-2015

Atmospheric Chemistry and Physics Discussions

Lidar observations of Nabro volcano aerosol layers in the stratosphere over Gwangju, Korea

D. Shin[1], D. Müller[2,3,4], K. Lee[5], S. Shin[2], Y. J. Kim[2], C. K. Song[1], and Y. M. Noh[2]

[1]National Institute of Environmental Research, Kyungseo-dong, Seo-gu, Incheon 404-708, South Korea
[2]School of Environmental Science & Engineering, Gwangju Institute of Science and Technology (GIST) Oryong-dong, Buk-gu, Gwangju 500-712, Korea
[3]Science Systems and Applications, Inc., MS 475 NASA Langley Research Center, Hampton, VA 23681, USA
[4]University of Hertfordshire, College Lane, Hatfield AL10 9AB, UK
[5]Department of Environmental Science & Engineering, Gwangju Institute of Science & Technology, Gwangju, South Korea

Received: 21 November 2014 – Accepted: 24 November 2014 – Published: 14 January 2015

Correspondence to: Y. M. Noh (nym@gist.ac.kr)

Published by Copernicus Publications on behalf of the European Geosciences Union.

Abstract

We report on the first Raman lidar measurements of stratospheric aerosol layers in the upper troposphere and lower stratosphere over Korea. The data were taken with the multiwavelength aerosol Raman lidar at Gwangju (35.10° N, 126.53° E), Korea. The volcanic ash particles and gases were released around 12 June 2011 during the eruption of the Nabro volcano (13.37° N, 41.7° E) in Eritrea, east Africa. Forward trajectory computations show that the volcanic aerosols were advected from North Africa to East Asia. The first observation of the stratospheric aerosol layers over Korea was on 19 June 2011. The stratospheric aerosol layers appeared between 15 and 17 km height a.s.l. The aerosol layers' maximum value of the backscatter coefficient and the linear particle depolarization ratio at 532 nm were $1.5 \pm 0.3\,\mathrm{Mm}^{-1}\,\mathrm{sr}^{-1}$ and 2.2 %, respectively. We found these values at 16.4 km height a.s.l. 44 days after this first observation, we observed the stratospheric aerosol layer again. We continuously probed the upper troposphere and lower stratosphere for this aerosol layer during the following 5 months, until December 2011. The aerosol layers typically occurred between 10 and 20 km height a.s.l. The stratospheric aerosol optical depth and the maximum backscatter coefficient at 532 nm decreased during these 5 months.

1 Introduction

Particles and trace gases which are injected into the stratosphere by volcanic eruptions are the biggest source of natural pollution in the stratosphere (Robock, 2000). One of the main components of gases from these eruptions are large amounts of sulfur dioxide (SO_2) which increases the optical thickness in stratospheric heights. These layers exert a cooling effect of Earth's atmosphere (Hofmann and Solomon, 1989) and influence chemical processes in the lower stratosphere (Rodriguez et al., 1991; Solomon et al., 1993). Stratospheric aerosols have notable impact on global climate because of their long residence time in the stratosphere and their large scale dispersion (Hofmann

et al., 2009). For example, the volcanic eruption of Mt. Pinatubo (15.14° N, 120.35° E) in the Philippines in 1991 injected approximately 20 Tg SO_2 into the stratosphere (Bluth et al., 1992; Guo et al., 2004) which led to a global-mean cooling effect of the troposphere by approximately 0.5–0.8 K in 1992 (McCormick et al., 1995; Parker et al., 1996). The integrated backscatter coefficient (at 532 nm) between the first tropopause height (approximately 15 km) to 33 km height a.s.l. decayed with an e-folding time of 1.14 and 1.29 years over Tsukuba (36.05° N, 140.13° E) and Naha (26.21° N, 127.69° E) in Japan, respectively (Uchino et al., 2012). Barnes and Hofmann (2001) reported that with regard to the integrated backscatter coefficient (at 532 nm) from 15.8 to 33 km height the Pinatubo aerosols in the stratosphere seemed to have returned to near background levels at Mauna Loa (19.53° N, 155.57° W) by mid 1996.

During the past 20 years, ground-based lidars have been demonstrated to be powerful methods for studying geometrical, optical, and microphysical characteristics of stratospheric aerosols (Wandinger et al., 1995; Ansmann et al., 2010; Mattis et al., 2010; Sawamura et al., 2012). In that regard, Raman lidar is particularly important as it allows for measuring extinction profiles as was shown for the first time by Ansmann et al. (1990). Despite these investigations, measurements of stratospheric aerosol properties under ambient conditions are still rare, and measurements are particularly sparse over Asian sites along the West Pacific Rim, or Ring of Fire (Uchino et al., 2012). In this paper, we report on observations of stratospheric aerosols over Gwangju (35.10° N, 126.53° E), Korea. The stratospheric aerosol layer originated from the Nabro eruption (13.37° N, 41.70° E) that occurred in Eritrea on 12 June 2011. To our knowledge, it is the first time that volcanic aerosols at stratospheric heights were observed with Raman lidar in Korea.

We present data on the temporal evaluation of the geometrical depth and integrated optical depth (at 532 nm) of the Nabro aerosol layer. Our observations add to data published by Sawamura et al. (2012) who observed the Nabro stratospheric layer with multiple lidar networks such as MPLNET (Welton et al., 2001), EARLINET (Pappalardo et al., 2014), and NDACC (http://www.ndsc.ncep.noaa.gov/) and independent

lidar groups and satellite CALIPSO (Cloud-Aerosol Lidar and Infrared Pathfinder Satellite Observation satellite) (Winker et al., 2009) in the Northern Hemisphere.

The lidar, the retrieval methods, and the trajectory modeling are presented in Sect. 2. The results of the trajectory modeling and the lidar data are presented in Sect. 3. The main findings of the lidar observations are summarized in Sect. 4.

2 Methodology

2.1 Lidar system MRS.LEA

We have been developing a novel multi-wavelength aerosol depolarization/Raman-quartz/water-vapor/spectrometer lidar system, dubbed MRS.LEA (Multi-wavelength Raman/Spectrometer Lidar in East Asia) since 2008. The instrument is used for the characterization of optical and microphysical properties of East Asian aerosols (Noh et al., 2008; Müller et al., 2010; Shin et al., 2010; Tatarov et al., 2011). The lidar station is located at the Gwangju Institute for Science and Technology (GIST), Republic of Korea (35.10° N, 126.53° E).

The light source of the lidar is a pulsed Nd:YAG laser (Surelite III-10, Continuum) which operates at the wavelength of 1064 nm. The pulse repetition rate is 10 Hz. A frequency-doubling crystal allows for generating linear-polarized laser light at 532 nm wavelength. In addition, frequency tripling generates laser light at 355 nm wavelength. In order to reduce the divergence of the emitted radiation, we use a beam expander at 532 and 1064 nm. The return signals are collected with a 14-inch Schmidt-Cassegrain telescope (C14, Celestron). The multi-wavelength Raman lidar measures elastically backscattered light at 355, 532 and 1064 nm, and backscattering from the Raman-shifted radiation (vibrational band of N_2) at 387 and 607 nm.

Hamamatsu R7400-20 photomultiplier tubes (PMT) are used to measure signals in the analog and photon-counting mode at the two 532 nm channels. We detect the parallel-polarized and cross–polarized backscatter signals, respectively. The bandwidth

of the interference filters is 1 at 532 nm (full width at half maximum = FWHM). A Hamamatsu R3236 PMT with a cooler is used for analog and photon-counting at 1064 nm. Transient recorders with 12-bit analog to digital converters and 250-MHz photon counters (TR 20-160, Licel) are used for processing the output signals of the PMTs.

The signal-to-noise ratio of the signals at 387 and 607 nm are comparably low in the stratosphere. We tried to optimize our analysis of the signals in the sense that we restricted our data analysis to the signals in the stratosphere.

2.2 Aerosol optical properties

We present data taken in the upper troposphere (UT) which extend to approximately 10 km height a.s.l. and the lower stratosphere (LS) which extends to approximately 24 km height a.s.l. The optical data products that describe the UT and LS aerosol layers were taken with our lidar system under cloud-free conditions during night-time. We had to apply long signal averaging times due to the low power of the emitted laser pulses. We performed signal-smoothing lengths of 400 m for the particle backscatter coefficients and the linear particle depolarization ratio. The Klett–Fernald method (Fernald, 1984; Klett, 1985) was used to determine particle backscatter coefficients. The calibration point of the backscatter profiles of the raw signals was set between approximately 28 and 30 km height a.s.l. where no particles but only molecules contributed to the measured signals.

We report the total stratospheric aerosol burden in terms of the stratospheric aerosol optical depth (AOD) at 532 nm wavelength for the height region from 10 to 24 km height a.s.l. The value of AOD significantly depends on the lidar ratio which is defined as the ratio of the particle extinction coefficient to the particle backscatter coefficient. Mattis et al. (2010) measured lidar ratios of 30–45 sr at 532 nm in the stratosphere. The data were taken between 2008 and 2009 over central Europe with a multiwavelength Raman lidar and describe stratospheric aerosols that originated from numerous eruptions of volcanoes on the Aleutian Islands, Kamchatka, Alaska, and the Kuril Islands. The aerosol layers typically occurred between 5 and 25 km height a.s.l. Based on the study

by Mattis et al. (2010) we chose an average lidar ratio of 38 sr at 532 nm. This value was used by Sawamura et al. (2012) for the analysis of their lidar observations of the Nabro aerosol layer.

We used radiosonde data to calculate the atmospheric molecular density from pressure and temperature profiles. Radiosondes were launched four times a day (00:00, 06:00, 18:00 and 24:00 UTC) at the Gwangju International Airport which is about 10 km away from our lidar site.

The linear particle depolarization ratio is useful to characterize the shape of the particles. We calculated the linear particle depolarization ratio δ^{p} at 532 nm according to the following equation (Biele et al., 2000; Freudenthaler et al., 2009):

$$\delta^{\mathrm{p}} = \frac{\beta^{\mathrm{m}}\left(\delta^{\mathrm{v}} - \delta^{\mathrm{m}}\right) + \beta^{\mathrm{p}}\delta^{\mathrm{v}}\left(1 + \delta^{\mathrm{m}}\right)}{\beta^{\mathrm{m}}\left(\delta^{\mathrm{m}} - \delta^{\mathrm{v}}\right) + \beta^{\mathrm{p}}\left(1 + \delta^{\mathrm{m}}\right)} \tag{1}$$

The linear volume depolarization ratio (particles plus molecules) is denoted by δ^{v}. The molecular and particle backscatter coefficient are denoted by β^{m} and β^{p}. The molecular (Rayleigh) depolarization ratio is denoted by δ^{m}. The molecular backscatter coefficient can be calculated from the radiosonde data.

The depolarization ratio of purely molecular backscattered signal is needed as input parameter for deriving the linear particle depolarization ratio. This value depends on the actual bandwidth of the interference filters of the lidar receiver as the bandwidth decides on whether the rotational Raman bands are included in the detected signals or not (Behrendt and Nakamura, 2002). We calculated a constant molecular depolarization ratio of 0.44 % which takes into account the actual bandwidth of the interference filter (more than 1 nm at the co-polarized and cross-polarized 532 nm) according to Behrendt and Nakamura (2002).

When measuring the depolarization ratio we need to consider the polarization-dependent receiver transmission factor. Backscatter signals are detected with different efficiencies because the transmission efficiency of the optical elements in the detector channels depends on the state of polarization of the incident light. This dependence

can lead to an under- or overestimation of the total signal that is detected (Mattis et al., 2009; Tesche et al., 2011). Therefore, we conducted transmission ratio measurements (Mattis et al., 2009) and applied them to our depolarization ratio calculation.

2.3 Air parcel trajectories computed with HYSPLIT and PRCF

The HYSPLIT (HYbrid Single-Particle Lagrangian Trajectory; version 4.9) forward trajectory modeling system (Draxler and Hess, 1997, 1998) was used to understand the spatial distribution of the transport pathway of the ash aerosol plume and to identify the potential receptor regions after the eruption of the Nabro volcano on 12 and 13 June 2011.

Global Data Assimilation System (GDAS) atmospheric fields were used in HYSPLIT to produce forward trajectories of air parcels originating from Mt. Nabro. The forward trajectories provided us with Lagrangian paths of air parcels in time steps of 1 h from 12 to 13 June 2011. This information was used to identify the potential receptor region and the transport pathway of the volcanic aerosol layer. Three-dimensional, 240 h forward trajectories departing from Mt. Nabro were calculated for every hour. The model used in our study uses a grid-cell size of $0.5^{\circ} \times 0.5^{\circ}$ and two different height maps which are from 0.5 to 10 km height a.s.l. and from 10 to 19 km height a.s.l. The trajectories were computed in time steps of 1 h from 12 (start time in 00:00 UTC) to 13 June 2011 (end time in 24:00 UTC).

We used PRCF (Potential Receptor Contribution Function) to identify the probable locations of receptors. The PRCF values for grid cells in the study domain were calculated by counting the trajectories not only ending at the cell but also crossing the cell. The PRCF value for the *ij*th cell is defined as a conditional probability, and n_{ij} is the number of segment trajectory endpoints *n* that fall into the *ij*th cell. To reduce the uncertainty in a grid cell with a small number of endpoints, an arbitrary weight function *w* was applied when the number of the end points in a particular cell was less than three times the average number of end points for all cells (Polissar et al., 2001). The

values of *w* were assigned as follows:

$$w = \begin{cases} 1.00, & 12 < n_{ij} \\ 0.7, & 6 < n_{ij} < 12 \\ 0.42, & 2 < n_{ij} < 6 \\ 0.17, & n_{ij} < 2 \end{cases} \quad (2)$$

3 Results and discussion

3.1 Computations of the transport of the Mt. Nabro volcanic aerosol plum

Mt. Nabro has an elevation of 2218 m a.s.l. The volcano is located at the border between Eritrea and Ethiopia in Northeast Africa near the Red Sea. The Infrared Atmospheric Sounding Interferometer (IASI) and the Smithsonian's Global Volcanism Program (SGVP 2011) reported the first activity of the Nabro eruption at 00:00 UTC on 12 June 2011. Visible plumes were rising to an altitude of 13 km a.s.l. and continued emissions were observed for several weeks. The volcanic aerosol plume was detected by the Moderate Resolution Imaging Spectrometer (MODIS) on the Aqua satellite at 10:45 UTC on 13 June 2011 (http://earthobservatory.nasa.gov). An estimated 1.3–2.0 Tg total mass of SO_2, ash, and water vapor were injected up to the stratosphere (Clarisse et al., 2012; Sawamura et al., 2012).

The distribution of PRCF in the study area is shown in Fig. 1. The PRCF map for emissions in the altitude range between 10 and 19 km height shows that grid cells with high PRCF values appeared mainly in East Asia. In contrast, the PRCF map for emissions from lower altitudes, i.e., in the altitude range between 0.5 and 10 km height shows grid cells with high PRCF values over Africa and India. This result means that the potential receptor areas are highly dependent on the vertical injection height of the volcanic material. In fact, an initial plume height of 9 to 14 km height a.s.l. was reported (based on the report of the Smithsonian Institution) and the main part of the volcanic

aerosol plume was injected into the UT and LS by the Asian anticyclone (Bourassa et al., 2012; Fairlie et al., 2014). Therefore volcanic emissions injected into higher altitudes could enter the measurement site over the Korean peninsula.

3.2 Vertical distribution of the stratospheric aerosol layers

We selected the nighttime measurements on 19 June 2011 and 8 August 2011 to study the optical properties and dispersion of the aerosol layers. The aerosol layers were detected for the first time on 19 June 2011, approximately 7 days after the eruption. CALIPSO observations showed the stratospheric aerosol layers in the UT and LS in South and South-East Asia approximately in the first 10 days after the eruption (Fairlie et al., 2014).

Figure 2 shows lidar measurements carried out from 16:00 to 18:00 UTC on 19 June 2011. We show profiles of the particle backscatter coefficient, the linear volume and the linear particle depolarization ratio, and meteorological parameters obtained from a radiosonde launched at 18:00 UTC. The aerosol layer shows a separation into two sub layers that stretch between 15 and 17 km height a.s.l. The peak value of the backscatter coefficient of the aerosol layer was $1.5 \pm 0.3\,\mathrm{M\,m^{-1}\,sr^{-1}}$ (532 nm) at 16.4 km height a.s.l.

The maximum value of the linear volume and the particle depolarization ratios were 1.9 and 2.2 % (532 nm) at 16.4 km height a.s.l., respectively. The mean value of the linear particle depolarization ratio of the aerosol layer is 1.58 %. This value is larger than what can be explained by molecular scattering which contributes approximately 0.44 % to the total signal. Stratospheric particles are usually assumed to be spherical (Mattis et al., 2010). Our result indicates that there was some contribution of non-spherical particles in the aerosol layer, i.e. glass- and mineral particles. We have insufficient information to provide a more detailed interpretation of this result.

We could not operate the lidar from 20 June to 2 August 2011 because of the arrival of the monsoon front, which usually is connected to strong clouds decks and heavy rain on a nearly daily basis.

Forty four days after our first measurement, we detected stratospheric aerosol layers that showed several peaks. Figure 2 shows an example of the measurement carried out on 3 August 2011. The layer thickness, according to the profiles of the particle backscatter coefficient was 9.5 km; the bottom of the layer was at 10 km and the top of the layer was at 19.5 km height a.s.l. This spread of the geometrical depth of the aerosol layer may be caused by vertical eddy diffusion in the stratosphere (Holton et al., 1995; Bitar et al., 2010). The stratospheric aerosol layers show a wavelength-dependence of the particle backscatter coefficient. The maximum value of the backscatter coefficient was $0.17 \pm 0.03\,\mathrm{M\,m^{-1}\,sr^{-1}}$ at 532 nm and $0.03 \pm 0.01\,\mathrm{M\,m^{-1}\,sr^{-1}}$ at 1064 nm at 17.5 km height a.s.l. The backscatter-related Ångström exponents (not shown) on average varied around 0.8–1.1 in this aerosol layer.

Slightly increased values of the linear particle depolarization ratio between 10 and 17 km height a.s.l. indicate the presence of non-spherical particles. The maximum value of the linear particle depolarization ratio was 1.9 % at 12 km height a.s.l. The aerosol layer seemed to be composed of spherical particles in the upper part of the aerosol layer and of non-spherical particles in the lower part of the aerosol layer. We observed this higher particle depolarization ratio in the lower part of the layer until the end of our measurement cycle (see Fig. 5). Sedimentation of glass- and mineral particles might be responsible for the higher depolarization ratios below 17 km height a.s.l. Again, we have insufficient information to give a more detailed interpretation of this result.

Figure 4 shows the time-height contour plot of the 532 nm range-corrected backscatter signals (logarithmic scale), and examples of vertical profiles of the particle backscatter coefficient and the linear particle depolarization ratio measured between 19 June and 7 October 2011. Gaps in the data were mostly the result of clouds that made it impossible to operate the lidar.

Figure 5 shows the temporal evolution of the aerosol optical depth (AOD) in the stratosphere over Gwangju and the maximum value of particle backscatter coefficient in the aerosol layer at 532 nm wavelength from June to December 2011. The stratospheric

AOD was computed from the particle backscatter coefficients at 532 nm, integrated from the bottom to the top of the aerosol layers (the 10 to 24 km height region) and assuming a lidar ratio of 38 sr.

The stratospheric aerosol layer was detected over Gwangju for the first time on 19 June, i.e., approximately 7 days after the eruption (see Fig. 3). This day defines the maximum value of 0.07 of AOD in the stratosphere. The maximum value of the particle backscatter coefficient was $1.5 \pm 0.3\,\mathrm{M\,m^{-1}\,sr^{-1}}$ at 532 nm.

The following day, a geometrically thin aerosol layer was observed between 16.5 and 18 km height a.s.l. The stratospheric AOD and the particle backscatter coefficient decreased sharply to 0.013 and $0.41\,\mathrm{M\,m^{-1}\,sr^{-1}}$, respectively. Then, from 3 August 2011 onward, we observed a variable stratospheric AOD. This result shows that the Nabro particles were distributed non-uniformly during June through June (Fairlie et al., 2014). AOD decreased with time until the end of the observation period. In contrast, the geometrical depth of the aerosol layer did not change significantly from 3 August 2011 (see Fig. 5). Our results are consistent with results presented by Sawamura et al. (2012) and Uchino et al. (2012). Sawamura et al. (2012) show the similar stratospheric AOD pattern were 0.023, 0.011, 0.023 and 0.010 on 22 June, 20, 22 July and 12 August 2011 at Hefei, China, respectively. Uchino et al. (2012) show that the integrated backscatter coefficient at 532 nm of the Nabro particles were distributed non-uniformly above the first tropopause height over Japan from June to early July, and almost uniformly after late July 2011. The integrated backscatter coefficients then decreased gradually from August to December 2011.

4 Summary and conclusions

We present for the first time results of Raman lidar observations of the temporal evolution of a stratospheric aerosol layer observed in the UT and LS over Korea. Particle backscatter coefficients and linear particle depolarization ratios, and the evolution of the vertical structure of the stratospheric aerosol layer were observed after the eruption of the Nabro volcano (Eritrea, East Africa) on 12 June 2011. We observed the aerosol layers for the first time on 19 June 2011. We continued with lidar observations three times per week from August until 14 December 2011. We could not carry out measurements after the first detection of the stratospheric layer until end of July because of the arrival of the monsoon front.

The stratospheric aerosols over Gwangju were located in a geometrically thin layer between 15 and 17 km height a.s.l. The maximum backscatter coefficient and the linear particle depolarization ratio were $1.5 \pm 0.3\,\mathrm{M\,m^{-1}\,sr^{-1}}$ and 2.2 % at 16.4 km height a.s.l., respectively, on 19 June 2011. The maximum backscatter coefficient and the aerosol optical depth of the stratospheric aerosol layer decreased during the 5 month observation period.

Sawamura et al. (2012) do not report on depolarization measurements that could help us determine whether or not ash particles were present. Uchino et al. (2012) report that non-spherical particles were seen in the lower regions of the layers until 24 September. However, in this study, the linear particle depolarization ratio showed also increased values in the lower part of the aerosol layer until the end of our measurement cycle. This result shows that non-spherical particles may have been present in the lower stratosphere for at least six months after the eruption on the volcano.

Our study adds to the limited information on volcanic aerosols over East Asia. It may also help in future observations of volcanic eruptions in East Asia, i.e. in source regions, which is part of the West Pacific Rim (Ring of Fire) where a large number of volcanic eruptions frequently occur. Lidar observations are very limited in this area.

Acknowledgements. This work was supported by a National Research Foundation of Korea (NRF) grant funded by the Korean government (MEST) (No.2012R1A1A2002983). This study was supported by the Ministry of Science and Technology, Korea, through the Institute of Science and Technology for Sustainability (UNU & GIST Joint Program). This work was funded by the Korea Meteorological Administration Research and Development Program under Grant CATER 2012-7080.

References

Ansmann, A., Riebesell, M., and Weitkamp, C.: Measurement of atmospheric aerosol extinction profiles with a Raman lidar, Opt. Lett., 15, 746–748, 1990.

Ansmann, A., Tesche, M., Groß, S., Freudenthaler, V., Seifert, P., Hiebsch, A., Schmidt, J., Wandinger, U., Mattis, I., and Müller, D.: The 16 April 2010 major volcanic ash plume over central Europe: EARLINET lidar and AERONET photometer observations at Leipzig and Munich, Germany, Geophys. Res. Lett., 37, L13810, doi:10.1029/2010GL043809, 2010.

Barnes, J. and Hofmann, D.: Variability in the stratospheric background aerosol over Mauna Loa Observatory, Geophys. Res. Lett., 28, 2895–2898, 2001.

Behrendt, A. and Nakamura, T.: Calculation of the calibration constant of polarization lidar and its dependency on atmospheric temperature, Opt. Express, 10, 805–817, 2002.

Biele, J., Beyerle, G., and Baumgarten, G.: Polarization lidar: correction of instrumental effects, Opt. Express, 7, 427–435, 2000.

Bitar, L., Duck, T., Kristiansen, N., Stohl, A., and Beauchamp, S.: Lidar observations of Kasatochi volcano aerosols in the troposphere and stratosphere, J. Geophys. Res.-Atmos. (1984–2012), 115, D00L13, doi:10.1029/2009JD013650, 2010.

Bluth, G. J., Doiron, S. D., Schnetzler, C. C., Krueger, A. J., and Walter, L. S.: Global tracking of the SO_2 clouds from the June, 1991 Mount Pinatubo eruptions, Geophys. Res. Lett., 19, 151–154, 1992.

Bourassa, A. E., Robock, A., Randel, W. J., Deshler, T., Rieger, L. A., Lloyd, N. D., Llewellyn, E. T., and Degenstein, D. A.: Large volcanic aerosol load in the stratosphere linked to Asian monsoon transport, Science, 337, 78–81, 2012.

Clarisse, L., Hurtmans, D., Clerbaux, C., Hadji-Lazaro, J., Ngadi, Y., and Coheur, P.-F.: Retrieval of sulphur dioxide from the infrared atmospheric sounding interferometer (IASI), Atmos. Meas. Tech., 5, 581–594, doi:10.5194/amt-5-581-2012, 2012.

Draxler, R. R. and Hess, G.: Description of the HYSPLIT4 Modeling System, NOAA Tech. Memo. ERL ARL-224, 24 pp., available at: http://www.arl.noaa.gov/web/models/hysplit4/win95/arl-224.pdf (last access: June 2014), 1997.

Draxler, R. R. and Hess, G.: An overview of the HYSPLIT_4 modelling system for trajectories, Aust. Meteorol. Mag., 47, 295–308, 1998.

Fairlie, T. D., Vernier, J.-P., Natarajan, M., and Bedka, K. M.: Dispersion of the Nabro volcanic plume and its relation to the Asian summer monsoon, Atmos. Chem. Phys., 14, 7045–7057, doi:10.5194/acp-14-7045-2014, 2014.

Fernald, F. G.: Analysis of atmospheric lidar observations: some comments, Appl. Optics, 23, 652–653, 1984.

Freudenthaler, V., Esselborn, M., Wiegner, M., Heese, B., Tesche, M., Ansmann, A., Müller, D., Althausen, D., Wirth, M., and Fix, A.: Depolarization ratio profiling at several wavelengths in pure Saharan dust during SAMUM 2006, Tellus B, 61, 165–179, 2009.

Guo, S., Bluth, G. J., Rose, W. I., Watson, I. M., and Prata, A.: Re-evaluation of SO_2 release of the 15 June 1991 Pinatubo eruption using ultraviolet and infrared satellite sensors, Geochem. Geophy. Geosy., 5, 1–31, doi:10.1029/2003GC000654, 2004.

Hofmann, D., Barnes, J., O'Neill, M., Trudeau, M., and Neely, R.: Increase in background stratospheric aerosol observed with lidar at Mauna Loa Observatory and Boulder, Colorado, Geophys. Res. Lett., 36, L15808, doi:10.1029/2009GL039008, 2009.

Hofmann, D. J. and Solomon, S.: Ozone destruction through heterogeneous chemistry following the eruption of El Chichon, J. Geophys. Res.-Atmos. (1984–2012), 94, 5029–5041, 1989.

Holton, J. R., Haynes, P. H., McIntyre, M. E., Douglass, A. R., Rood, R. B., and Pfister, L.: Stratosphere–troposphere exchange, Rev. Geophys., 33, 403–439, 1995.

Klett, J. D.: Lidar inversion with variable backscatter/extinction ratios, Appl. Optics, 24, 1638–1643, 1985.

Müller, D., Mattis, I., Tatarov, B., Noh, Y., Shin, D., Shin, S., Lee, K., Kim, Y., and Sugimoto, N.: Mineral quartz concentration measurements of mixed mineral dust/urban haze pollution plumes over Korea with multiwavelength aerosol Raman-quartz lidar, Geophys. Res. Lett., 37, L20810, doi:10.1029/2010GL044633, 2010.

Mattis, I., Tesche, M., Grein, M., Freudenthaler, V., and Müller, D.: Systematic error of lidar profiles caused by a polarization-dependent receiver transmission: quantification and error correction scheme, Appl. Optics, 48, 2742–2751, 2009.

Mattis, I., Siefert, P., Müller, D., Tesche, M., Hiebsch, A., Kanitz, T., Schmidt, J., Finger, F., Wandinger, U., and Ansmann, A.: Volcanic aerosol layers observed with multiwavelength Raman lidar over central Europe in 2008–2009, J. Geophys. Res.-Atmos. (1984–2012), 115, D00L04, doi:10.1029/2009JD013472, 2010.

McCormick, M. P., Thomason, L. W., and Trepte, C. R.: Atmospheric effects of the Mt Pinatubo eruption, Nature, 373, 399–404, 1995.

Noh, Y. M., Kim, Y. J., and Müller, D.: Seasonal characteristics of lidar ratios measured with a Raman lidar at Gwangju, Korea in spring and autumn, Atmos. Environ., 42, 2208–2224, 2008.

Pappalardo, G., Mona, L., D'Amico, G., Wandinger, U., Adam, M., Amodeo, A., Ansmann, A., Apituley, A., Alados Arboledas, L., Balis, D., Boselli, A., Bravo-Aranda, J. A., Chaikovsky, A., Comeron, A., Cuesta, J., De Tomasi, F., Freudenthaler, V., Gausa, M., Giannakaki, E., Giehl, H., Giunta, A., Grigorov, I., Groß, S., Haeffelin, M., Hiebsch, A., Iarlori, M., Lange, D., Linné, H., Madonna, F., Mattis, I., Mamouri, R.-E., McAuliffe, M. A. P., Mitev, V., Molero, F., Navas-Guzman, F., Nicolae, D., Papayannis, A., Perrone, M. R., Pietras, C., Pietruczuk, A., Pisani, G., Preißler, J., Pujadas, M., Rizi, V., Ruth, A. A., Schmidt, J., Schnell, F., Seifert, P., Serikov, I., Sicard, M., Simeonov, V., Spinelli, N., Stebel, K., Tesche, M., Trickl, T., Wang, X., Wagner, F., Wiegner, M., and Wilson, K. M.: Four-dimensional distribution of the 2010 Eyjafjallajökull volcanic cloud over Europe observed by EARLINET, Atmos. Chem. Phys., 13, 4429–4450, doi:10.5194/acp-13-4429-2013, 2013.

Parker, D., Wilson, H., Jones, P. D., Christy, J., and Folland, C. K.: The impact of Mount Pinatubo on world-wide temperatures, Int. J. Climatol., 16, 487–497, 1996.

Polissar, A. V., Hopke, P. K., and Harris, J. M.: Source regions for atmospheric aerosol measured at Barrow, Alaska, Environ. Sci. Technol., 35, 4214–4226, 2001.

Robock, A.: Volcanic eruptions and climate, Rev. Geophys., 38, 191–219, 2000.

Rodriguez, J. M., Ko, M. K., and Sze, N. D.: Role of heterogeneous conversion of N_2O_5 on sulphate aerosols in global ozone losses, Nature, 352, 134–137, 1991.

Sawamura, P., Vernier, J.-P., Barnes, J., Berkoff, T., Welton, E., Alados-Arboledas, L., Navas-Guzmán, F., Pappalardo, G., Mona, L., and Madonna, F.: Stratospheric AOD after the 2011 eruption of Nabro volcano measured by lidars over the Northern Hemisphere, Environ. Res. Lett., 7, 034013, doi:10.1088/1748-9326/7/3/034013, 2012.

Shin, D., Noh, Y., Tatarov, B., Shin, S., Kim, Y., and Müller, D.: Multiwavelength aerosol Raman LIDAR for optical and microphysical aerosol typing over East Asia, 25th International Laser Radar Conference, 5–9 July 2010, St.-Petersburg, Russia, 2010.

Smithsonian Institution: Global Volcanism Program; available at: http://volcano.si.edu/world/volcano.cfm?vnum=0201-101&volpage=var (last access: July 2012), 2014.

Solomon, S., Sanders, R., Garcia, R., and Keys, J.: Increased chlorine dioxide over Antarctica caused by volcanic aerosols from Mount Pinatubo, Nature, 363, 245–248, 1993.

Tatarov, B., Müller, D., Shin, D. H., Shin, S. K., Mattis, I., Seifert, P., Noh, Y. M., Kim, Y., and Sugimoto, N.: Lidar measurements of Raman scattering at ultraviolet wavelength from mineral dust over East Asia, Opt. Express, 19, 1569–1581, 2011.

Tesche, M., Gross, S., Ansmann, A., Mueller, D., Althausen, D., Freudenthaler, V., and Esselborn, M.: Profiling of Saharan dust and biomass-burning smoke with multiwavelength polarization Raman lidar at Cape Verde, Tellus B, 63, 649–676, 2011.

Uchino, O., Sakai, T., Nagai, T., Nakamae, K., Morino, I., Arai, K., Okumura, H., Takubo, S., Kawasaki, T., Mano, Y., Matsunaga, T., and Yokota, T.: On recent (2008–2012) stratospheric aerosols observed by lidar over Japan, Atmos. Chem. Phys., 12, 11975–11984, doi:10.5194/acp-12-11975-2012, 2012.

Wandinger, U., Ansmann, A., Reichardt, J., and Deshler, T.: Determination of stratospheric aerosol microphysical properties from independent extinction and backscattering measurements with a Raman lidar, Appl. Optics, 34, 8315–8329, 1995.

Welton, E. J., Campbell, J. R., Spinhirne, J. D., and Scott III, V. S.: Global monitoring of clouds and aerosols using a network of micropulse lidar systems, Proc. SPIE, 4153, 151–158, doi:10.1117/12.417040, 2001

Winker, D. M., Vaughan, M. A., Omar, A., Hu, Y., Powell, K. A., Liu, Z., Hunt, W. H., and Young, S. A.: Overview of the CALIPSO mission and CALIOP data processing algorithms, J. Atmos. Ocean. Tech., 26, 2310–2323, 2009.

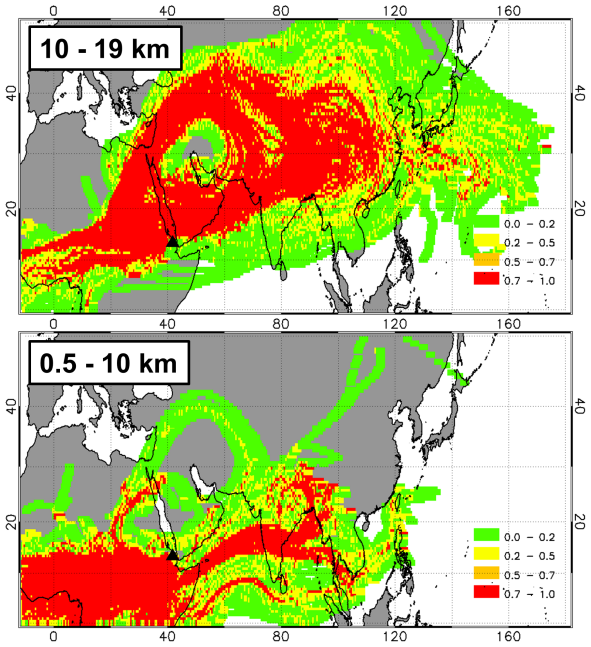

Figure 1. Potential receptor contribution function (PRCF) maps for transport identification of the plume from the Nabro volcano (black solid triangle). The air parcels were released in the altitude range between 10 and 19 km height a.s.l. (top) and between 0.5 and 10 km height a.s.l. (bottom) in time steps of 1 h from 12 to 13 June 2011. Colors indicate high potential receptor areas.

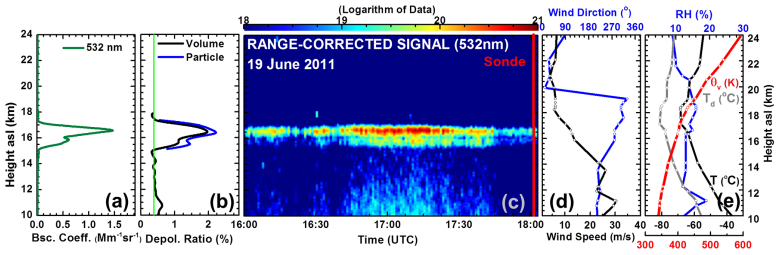

Figure 2. The stratospheric aerosol layer observed from 16:00 to 18:00 UTC on 19 June 2011. The two left panels show the particle backscatter coefficient at 532 nm **(a)** and the linear volume and particle depolarization ratio at 532 nm **(b)**. The green vertical line in **(b)** indicates the molecular depolarization ratio of 0.44 % at 532 nm. The middle panel shows the aerosol layer in terms of the 532 nm range-corrected backscatter signal (in arbitrary units) as a function of height and time **(c)**. The red line in **(c)** indicates the time of the radiosonde launch (at 18:00 UTC). The two right panels show the radiosonde profiles. Wind speed and wind direction are shown in **(d)**. Relative humidity (RH), dew point (T_d), temperature (T) and virtual potential temperature (θ_v) are shown in **(e)**.

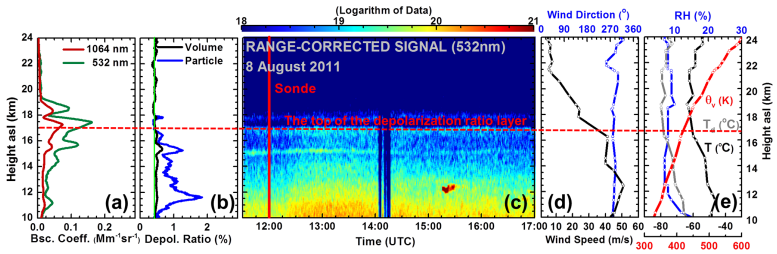

Figure 3. Same as Fig. 2 except for the measurement period from 11:30 to 17:00 UTC on 8 August 2011. Meteorological parameters (**c** and **d**) were measured with a radiosonde launched at 12:00 UTC.

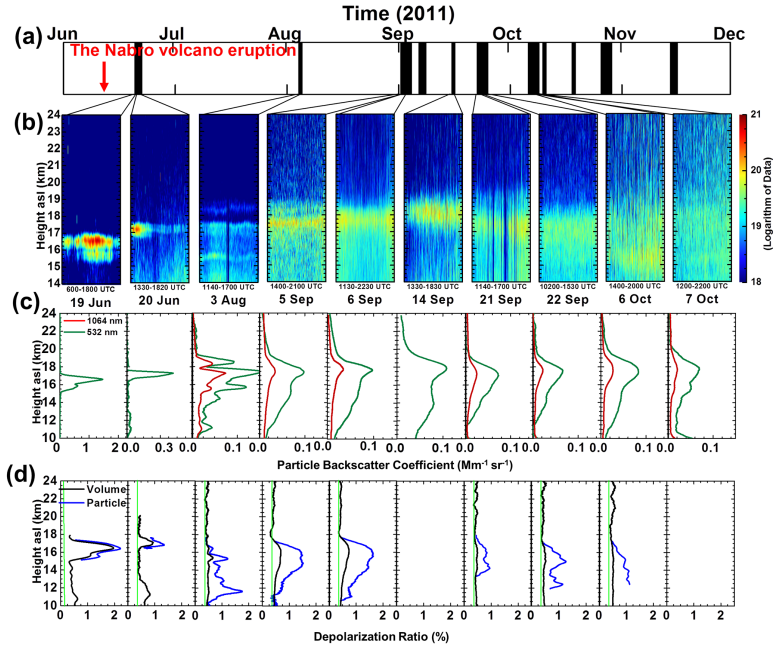

Figure 4. (a) Time series of measurements taken between 19 June and 7 October 2011. **(b)** Contour plot (time-height) of the 532-nm range-corrected backscatter signal. **(c)** Profiles of the particle backscatter coefficient at 532 and 1064 nm. **(d)** Profiles of the linear particle depolarization ratio and the total depolarization ratio (particles plus molecules) at 532 nm. Because of low signal-to-noise ratios of the cross-polarized signals at 532 nm, profiles of the linear particle depolarization ratio are not shown for the measurements carried out on 14 September and 7 October 2011.

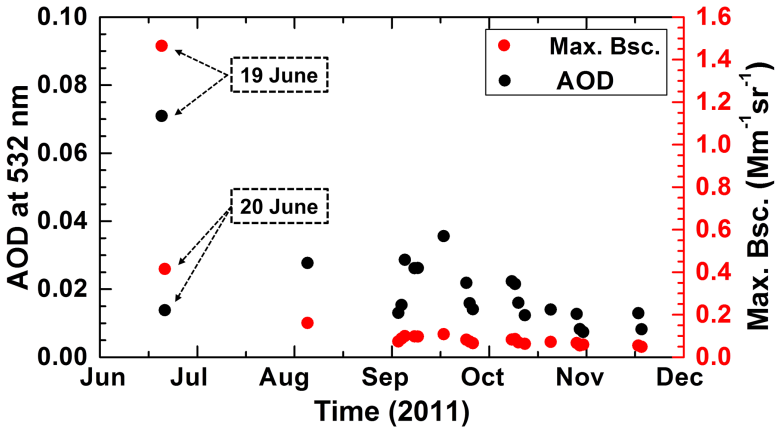

Figure 5. Temporal variation of the stratospheric aerosol optical depth (AOD) at 532 nm (closed black circles) of the stratospheric aerosol layers and the maximum backscatter coefficient at 532 nm (closed red circles).